




Physical adsorption and oxidation of ultra-thin MoS₂ crystals: insights into surface engineering for 2D electronics and beyond

Yingchun Jiang¹ , Zihan Liu¹ , Huimin Zhou², Anju Sharma³,
Jia Deng² and Changhong Ke^{1,4} 

¹ Department of Mechanical Engineering, State University of New York at Binghamton, Binghamton, NY 13902, United States of America

² Department of Systems Science and Industrial Engineering, State University of New York at Binghamton, Binghamton, NY 13902, United States of America

³ Small Scale Systems Integration and Packaging Center, State University of New York at Binghamton, Binghamton, NY 13902, United States of America

⁴ Materials Science and Engineering Program, State University of New York at Binghamton, Binghamton, NY 13902, United States of America

E-mail: cke@binghamton.edu

Received 27 April 2023, revised 21 June 2023

Accepted for publication 26 June 2023

Published 18 July 2023



CrossMark

Abstract

The oxidation mechanism of atomically thin molybdenum disulfide (MoS₂) plays a critical role in its nanoelectronics, optoelectronics, and catalytic applications, where devices often operate in an elevated thermal environment. In this study, we systematically investigate the oxidation of mono- and few-layer MoS₂ flakes in the air at temperatures ranging from 23 °C to 525 °C and relative humidities of 10%–60% by using atomic force microscopy (AFM), Raman spectroscopy and x-ray photoelectron spectroscopy. Our study reveals the formation of a uniform nanometer-thick physical adsorption layer on the surface of MoS₂, which is attributed to the adsorption of ambient moisture. This physical adsorption layer acts as a thermal shield of the underlying MoS₂ lattice to enhance its thermal stability and can be effectively removed by an AFM tip scanning in contact mode or annealing at 400 °C. Our study shows that high-temperature thermal annealing and AFM tip-based cleaning result in chemical adsorption on sulfur vacancies in MoS₂, leading to p-type doping. Our study highlights the importance of humidity control in ensuring reliable and optimal performance for MoS₂-based electronic and electrochemical devices and provides crucial insights into the surface engineering of MoS₂, which are relevant to the study of other two-dimensional transition metal dichalcogenide materials and their applications.

Supplementary material for this article is available [online](#)

Keywords: transition metal dichalcogenide, monolayer molybdenum disulfide, physical adsorption, oxidation mechanism, surface engineering

(Some figures may appear in colour only in the online journal)

1. Introduction

Two-dimensional (2D) transition metal dichalcogenides (TMDs) have received increasing research attention as building blocks for the next generation of nanoelectronics and optoelectronics. Ultra-thin molybdenum disulfide (MoS₂) is

particularly promising because of its band gap of 1.8 eV, high room temperature on/off current ratios of 1×10^8 , high electron mobilities of up to $200 \text{ cm}^2 \text{ V}^{-1} \text{ s}^{-1}$ [1, 2] and superior bending rigidities [3]. These remarkable material properties enable many applications, such as photovoltaics and photodetectors [4, 5], chemical sensors [6, 7], and

electrochemical catalysts [8–10]. However, nanoelectronics fabrication typically involves thermal annealing to remove contaminants or to tune the electrical properties [11, 12], and operating nanoelectronics often generate Joule heating, causing a temperature rise of up to $\sim 250^\circ\text{C}$ [13]. The elevated thermal environment can have detrimental effects on the electrical [14, 15] and mechanical properties [16] of the material, which challenges the stability and reliability of TMDs-based devices. On the other hand, thermal annealing of MoS₂ is a facile and cost-effective approach for fabricating p-type field effect transistors [17, 18], electrochemical sensing applications [8, 19, 20], and electrocatalysts for hydrogen-evolution reactions [9, 10, 21], etc. Therefore, a full understanding of the thermal oxidation mechanism of MoS₂ is essential to ensure the reliability and optimal performance of MoS₂-based devices.

Prior research on the surface oxidation of MoS₂ was focused on creating more active sites (e.g. etch pits and cracks) to modulate its electronic structural and electrical properties through plasma-assisted etching [22, 23] and thermal treatment in the air [24, 25] or in oxygen [26–28]. The oxidation threshold of MoS₂ was found in the range of 250°C – 400°C , accompanied by the formation of triangular etch pits [25, 27, 29], cracks [30], and molybdenum oxides [31, 32]. The researchers directly heated the MoS₂ samples to or above the oxidation temperature, but the morphological and chemical structural evolutions at lower temperatures were little explored. Other studies reported enhanced photoluminescence by the physical adsorption of O₂ and H₂O molecules on MoS₂ flakes, which can be reversed by vacuum pumping [30, 33, 34]. Energy dispersive x-ray spectroscopy (XPS) measurements and Auger electron spectroscopy studies have detected substantial amounts of physically adsorbed oxygen on the surface of MoS₂ flakes after annealing in the air [35]. Nevertheless, the effects of the physically adsorbed substances on the oxidation of MoS₂ remain elusive.

In this study, we systematically investigate the oxidation of mono- and few-layer MoS₂ under a wide temperature range of 23°C – 525°C in the air using atomic force microscopy (AFM), Raman spectroscopy, and XPS measurements. We reveal, *for the first time*, the formation of a uniform nanometer-thick physical adsorption layer and nanoparticles on the basal plane of atomically thin MoS₂ in the air with a relative humidity (RH) of $\sim 60\%$, and their evolution with increasing annealing temperature. Our study shows this physical adsorption layer acts as a thermal shield of the underlying MoS₂ lattice to enhance its thermal stability. Finally, we investigate the formation mechanisms of the physical adsorption layer by repeated AFM tip-based cleaning and thermal annealing in humid ($\sim 60\%$ RH) and dry ($\sim 10\%$ RH) air. Our finding suggests a facile and effective method to modify the surface properties of atomically thin MoS₂. Our study provides insights into the surface engineering of MoS₂ that are relevant to the study of other 2D-TMDs and their applications.

2. Results and discussion

2.1. Physical adsorption on MoS₂

To observe the evolution of the oxidation process of pristine MoS₂, mechanically exfoliated MoS₂ flakes supported on SiO₂/Si substrate were step-wise heated at an increment of 50°C . Figures 1(a)–(d) shows the morphology evolution of a MoS₂ flake that contains monolayer (1L), bilayer (2L), and trilayer (3L) regions (referred to as 1L–3L MoS₂ flake) by non-contact mode (NCM) imaging. The 1L–3L MoS₂ flake maintains its global morphology at up to 300°C in air (see figure S1(g) in the supplemental information), but undergoes severe sublimation and forms triangular etch pits at 400°C . These results are generally consistent with prior annealing studies of MoS₂ crystals [11, 27, 29]. However, contrary to a report that MoS₂ crystals remain intact at 350°C [36], our high-resolution AFM measurements reveal clear oxidation signs, such as the noticeably enlarged crack gap (indicated by the red arrow in figures 1(a)–(c)) and sublimation along the flake boundary and layer steps (figures 1(c) and S2).

Figures 1(e)–(f) reveals the formation of nanoparticles on the surface of the MoS₂ flake, which may initiate at a temperature as low as 150°C (also see figure S2(d), figures S3(k)–(l)). They grow in volume and density with increasing annealing temperature and reach the maximum surface coverage after 250°C , then start to shrink at 300°C , and finally vanish at 350°C (figures S2 and S3). These nanoparticles formed below 300°C are deemed as physical adsorbates and can be easily removed using an AFM tip, which is discussed in a later section. The larger nanoparticles found at step edges of the 1L to the 2L region and the 2L to the 3L region at 400°C , which are indicated by the red and blue dashed lines in figure 1(c), are likely residuals of molybdenum oxides (MoO_x) caused by inadequate sublimation [23]. While these MoO_x particles grow in size and quantity under extended annealing (figure 1(d)), they may survive even a temperature of 525°C (figure S4) and are difficult to remove using an AFM tip.

Furthermore, in contrast to a prior report that the thickness of atomically thin MoS₂ does not change after oxidation treatment below 340°C [27], figure 1(g) shows that the thickness of the 1L, 2L, and 3L regions increases by 1.06, 1.19, and 1.23 nm, respectively, after annealing at 350°C . These noticeable height increases are likely because of the physical adsorption of ambient moisture, which forms a uniform nanometer-thick layer on top of the MoS₂ flake. Two observations support that hypothesis: (i) the full width at half maximum (FWHM) and the Raman peak intensities of this flake remain nearly unchanged as the annealing temperature ramps up to 350°C , indicating that the crystalline structure of the MoS₂ flake remains intact after annealing at 350°C (figure S5); (ii) the NCM phase image shows phase contrast changes with increasing annealing temperature, which indicates the changing surface properties (figure S6).

Figure 1(h) shows that the step height from the 1L to the 2L regions increases by $\sim 25.5\%$ after annealing at 350°C , whereas the step height from the 2L to the 3L regions

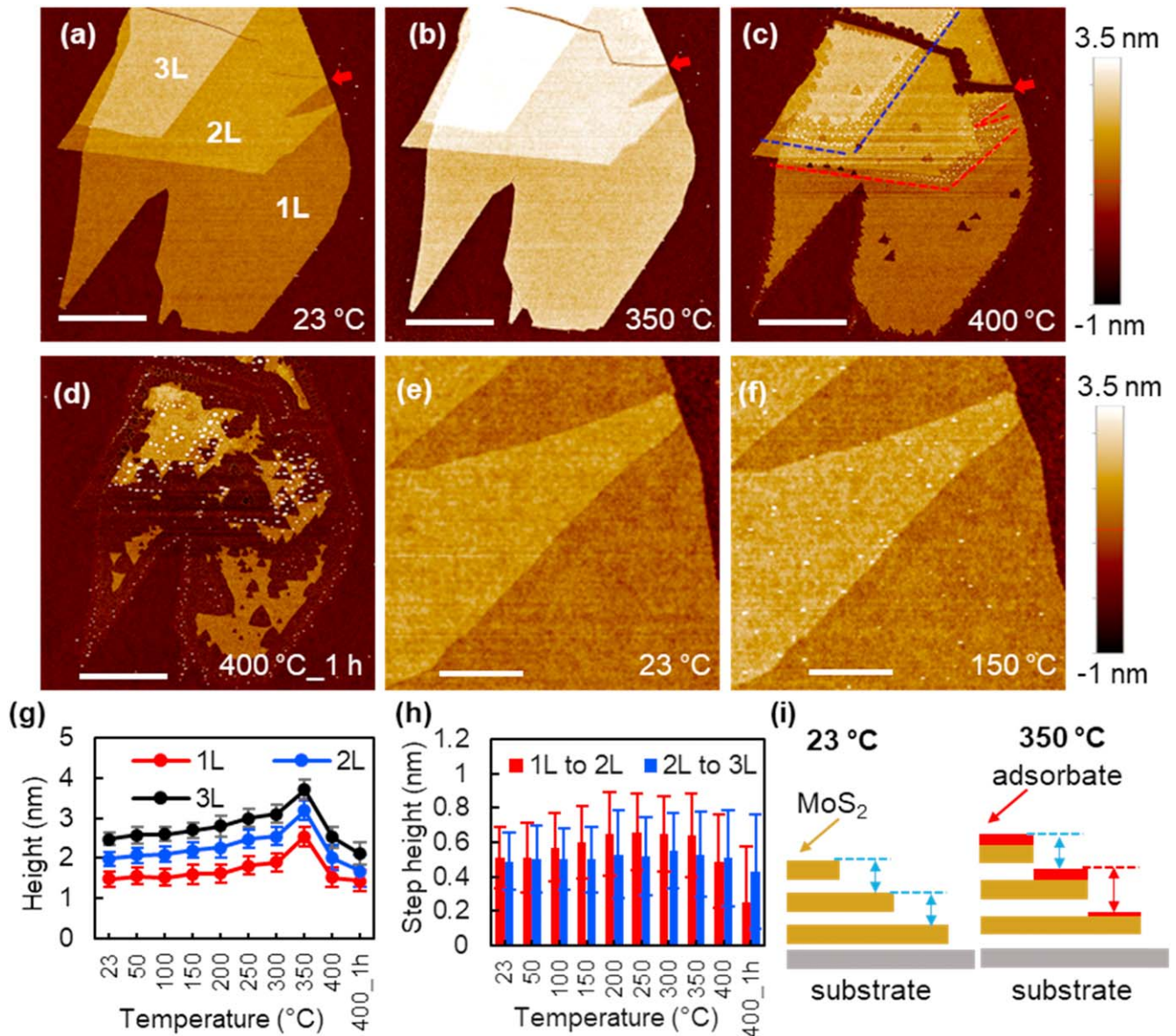


Figure 1. Morphology and layer-thickness (height) evolution of one 1L–3L MoS₂ flake before (23 °C) and after annealing (50 °C–400 °C) in the air with ~60% RH. Selected AFM topography images of the flake (a) before annealing, after annealing at (b) 350 °C and (c) 400 °C for 15 min, and (d) after annealing at 400 °C for 1 h. Scale bar, 3 μm. (e) and (f) zoom-in scans before annealing and after annealing at 150 °C for 15 min. Scale bar, 500 nm. (g) The evolution of the layer-thickness for the monolayer (1L), bilayer (2L), and trilayer (3L) regions. (h) The evolution of the step height between the neighboring domains. (i) A schematic diagram of the layer-thickness evolution due to physical adsorption. The error bars represent the standard error of at least four independent measurements for each type of specimen.

increases by ~8.2%. The noticeable difference in step height increase can be explained using the simplified model shown in figure 1(i). The adsorption layer is thinner on the 1L region because of the passivation effect of the substrate [37]. The adsorbed substances on the 2L and 3L regions have nearly the same build-up rate and thus thickness, as compared with the slower adsorption rate on the 1L region. Therefore, the height difference between the 2L and 3L regions remains almost unchanged, while the step height between the 1L and 2L regions substantially increases with the annealing temperature.

Complementary to the morphology and thickness evolutions, the effect of annealing on the MoS₂ crystal structure was investigated through *ex situ* Raman

spectroscopy, with a focus on crystalline quality, doping level, and tensile strain. As figure 2 shows, the A_{1g} mode upshifts and narrows with increasing annealing temperature above 200 °C. This is consistent with a prior study on oxygen treatment of MoS₂ [27]. Figures 2(a)–(c) shows that the maximum upshifts for the A_{1g} peak for 1L, 2L and 3L MoS₂ are 0.48, 1.03 and 0.29 cm⁻¹, respectively. Correspondingly, the decrease in FWHM, shown in figures 2(d)–(f), is 0.31, 1.2, and 0.69 cm⁻¹, respectively.

The mechanically exfoliated MoS₂ flakes often contain naturally occurring sulfur vacancies [38], which act as electron donors, resulting in the n-type doping of MoS₂ [1]. These electron donors interact strongly with the phonon of the A_{1g} mode, leading to the softening and broadening of the

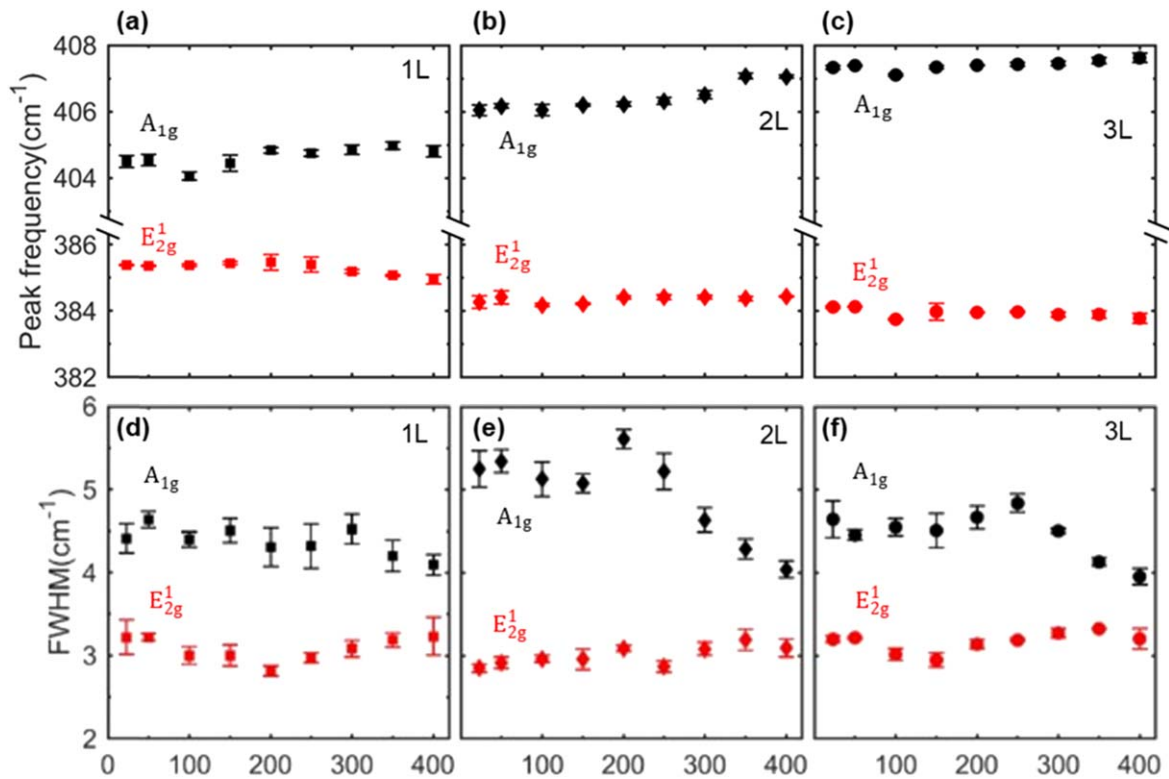


Figure 2. The *ex situ* Raman spectra of the 1L–3L MoS₂ flake shown in figure 1. (a)–(c) Raman peak frequencies of the A_{1g} (black markers) and E_{2g}¹ (red markers) modes, (d)–(f) Full width at half maximum (FWHM) of the two modes for the 1L (square markers), 2L (diamond markers), and 3L (circle markers) regions as a function of annealing temperature. Error bars are quantified as standard deviation calculated from three to five measurements for each region.

mode [39]. Thermal annealing can accelerate the chemical adsorption of oxygen atoms on the sulfur vacancies, leading to the depletion of electrons and resulting in p-type doping [40]. Therefore, the stiffening and narrowing of the A_{1g} mode with temperature can be attributed to annealing-induced p-type doping of MoS₂. In contrast, the E_{2g}¹ mode is less sensitive to doping [39], but more sensitive to applied strain [41]. Thus, the slight down-shifting of the E_{2g}¹ mode ($\sim 0.4 \text{ cm}^{-1}$) is a result of stress relaxation (figures 2(a)–(c)).

The flake height and the upshift of the A_{1g} band peak after annealing at 350 °C. After heating at 400 °C for 15 min, the heights of the 1L–3L flake decrease to their original levels, while the FWHM of the A_{1g} mode decreases below its original level. These results indicate that the physical adsorption layer that causes the height increase of MoS₂, can be removed by annealing in air at 400 °C for 15 min or less, while the chemical adsorption, which leads to p-type doping, cannot be reversed by thermal annealing.

To better understand the physical adsorption phenomenon, we conducted two rounds of thermal annealing at 240 °C, each followed by an AFM tip-based cleaning, and then final annealing at 400 °C for 3 h on a 2L–3L MoS₂ flake. The AFM topography image of the flake after each process is shown in figures 3(a)–(e). Figure 3(f) illustrates the AFM tip-based cleaning process. By scanning the surface of the annealed MoS₂ flakes with an AFM tip in contact mode, the tip breaks the continuity of the physical adsorption layer, causing the adsorbates to be pushed away and pile up on the

substrate along the scan direction, as evidenced by the tall (white) features around the edges of the dashed boxes in figure 3(b). Figure 3(g) shows that thermal annealing at 240 °C increases the height and surface roughness of the 3L and 2L regions, while the AFM tip-based cleaning restores them. More discussions comparing the tip-cleaned and uncleaned MoS₂ regarding its topography, phase contrast, and lateral force response can be found in figures S7–S9.

The integrity of the 3L MoS₂ crystal lattice is preserved after annealing and tip-based cleaning, as shown by the intact Raman peak positions (figure 3(h)) and similar optical contrast between the cleaned and uncleaned regions (inset in figure 3(d)). However, the FWHM of the A_{1g} mode decreases by 5% and 12% after the first- and second-round AFM tip-based cleaning, respectively, likely because of the filling of pre-existing or newly formed sulfur vacancies by oxygen atoms through chemical adsorption, resulting in p-type doping of the MoS₂. The tip-based cleaning of the adsorption layer on MoS₂ can result in more sulfur vacancies, as sulfur atoms can be removed along with adsorbates [41]. On the other hand, the E_{2g}¹ band is unaffected, indicating negligible residual strains in the MoS₂ flake.

The results obtained from the repeated thermal annealing and tip-based cleaning processes indicate that (i) a uniform nanometer-thick physical adsorption layer forms on the basal plane of MoS₂ when annealed in humid air at 240 °C, and (ii) AFM tip-based cleaning is capable of removing this physical

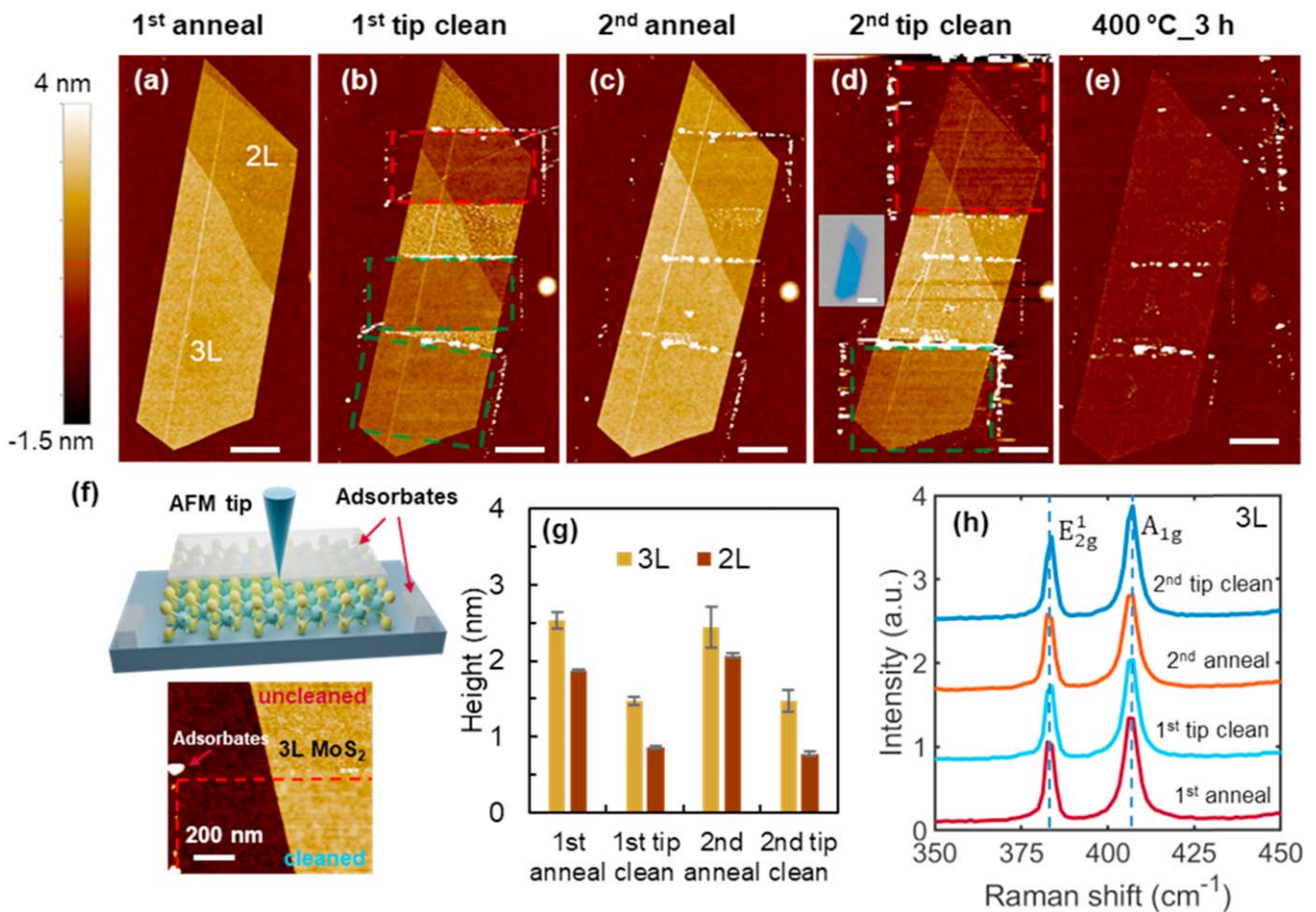


Figure 3. Sequential thermal annealing of a 2L–3L MoS₂ flake at 240 °C and 400 °C in the air under ~60% RH and AFM tip-based cleaning of the physical adsorption layer. AFM topography images of the flake after (a) the first annealing at 240 °C and (b) AFM tip-based cleaning, after the second (c) annealing at 240 °C and (d) tip-based cleaning, (e) after annealing at 400 °C for 3 h. The green and red dashed boxes in (b) and (d) mark the 3L and 2L regions cleaned by the AFM tip, respectively. The inset in (d) shows an optical image after the second tip-based cleaning. Scale bar, 1 μm. (f) Schematic of the AFM tip-based cleaning process of the physical adsorption layer on MoS₂. (g) Height changes of the 2L and 3L regions after sequential annealing and tip cleaning. The error bars represent the standard deviation of measurements taken on three different regions with an average area of ~60 μm². (h) Raman spectra of the 3L region recorded after each annealing or cleaning procedure.

adsorption layer and altering the surface properties of MoS₂ by introducing more sulfur vacancies.

2.2. Ice-like dendritic features

A pristine 2L MoS₂ flake is burned out with large MoO₃ particles as residual ashes after annealing at 400 °C for 3 h (figures S10(a)–(c)). In comparison, for a pre-annealed 2L–3L MoS₂ flake at 240 °C that is subjected to the same annealing conditions, a ~0.8 nm thick layer remains on the substrate (figures S10(d)–(f)). This suggests that the presence of the uniform physical adsorption layer on the pre-annealed MoS₂ flake acts as a thermal protection layer for the underlying MoS₂ crystal lattices.

Figures 4(a)–(c) shows that a pre-annealed 2L MoS₂ flake is free of visible etch pits after annealing at 330 °C for 10 h, which contrasts with prior reports that a fresh 2L MoS₂ is entirely thinned down to 1L under the same annealing condition [29] and numerous etch pits formed on the 1L–4L MoS₂ flakes after annealing at 320 °C for merely 3 h [27].

The Raman spectra on the center of the flake do not show visible changes after annealing at 330 °C for 10 h (figure 4(g)), indicating that the central region of the 2L MoS₂ flake remains intact. After a total of 14 h annealing (figure 4(d)), the intensities of both Raman modes reduce drastically and the corresponding peak frequency difference reduces from 21.7 to 20.4 cm⁻¹ (figure 4(g)), suggesting that the 2L region is thinned down to 1L. It is noted that the Raman peak difference for the thermally-thinned 1L MoS₂ remains larger than that of a pristine monolayer MoS₂ (~18 cm⁻¹) [42, 43], likely because of the slight blue shift of the A_{1g} mode that is caused by oxidation-induced p-type doping [25, 29, 44]. The findings of the intact structure without noticeable signs of structural damages (e.g. etching pits) and the prolonged survival time at 330 °C suggest that the physical adsorption layer acts as a thermal shield for the underlying MoS₂ crystal lattice and slows etch site growth, improving the stability and durability of the MoS₂ flake.

Figures 4(c)–(e) shows ice-like dendritic features and MoO_x particles on the flake. After annealing for 10 h and 14 h,

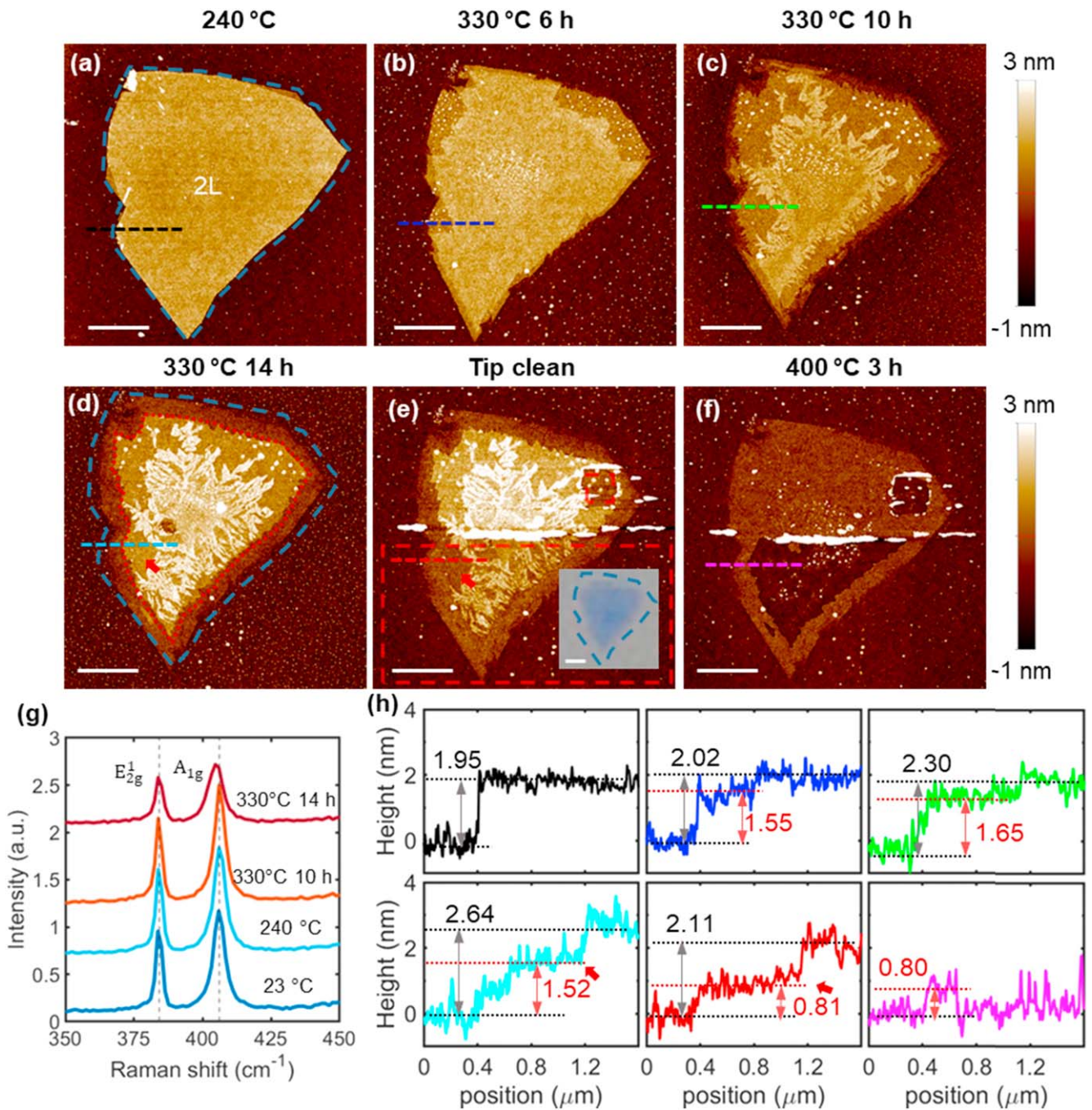


Figure 4. Thermal annealing of a 2L MoS₂ flake in the air under $\sim 60\%$ RH and AFM tip-based cleaning. AFM topography images of the flake after annealing at (a) 240 °C, (b)–(d) 330 °C for (b) 6 h, (c) 10 h, (d) 14 h, (e) after the AFM tip-based cleaning of the region marked by red dashed boxes (inset shows the optical image), (f) after annealing at 400 °C for 3 h. Scale bars, 1 μm . The light blue dashed lines in (d), (e) mark the original edge of the flake while the red dashed line in (e) marks the edge of the remaining MoS₂ flake. (g) Selected Raman spectra recorded around the center of the flake. (h) Flake height profiles along the dashed lines in (a)–(f).

the heights of these dendritic features are measured to be about 0.7 nm and 1.1 nm, respectively (figure 4(h)). Those dendritic features and nanoparticles are mechanically robust and adhere well to the substrate, and cannot be removed by blowup with compressive air or using an AFM tip with an applied normal force of up to 20 nN (figure 4(e)). In comparison, the AFM tip-based cleaning can remove a layer of materials of about 0.71 nm in thickness from the thermally thinned-down MoS₂ region (indicated by red arrows in figures 4(d)–(h)). Our phase

images further confirm that the AFM tip-based cleaning removes an adsorption layer formed during cooling (figure S11). The Raman spectra of the cleaned region (figures S12, S13) show that the A_{1g} band downshifts and broadens, suggesting disordering or amorphization of the MoS₂ crystal [45]. This observation suggests that the AFM tip removes the loosely bonded p-type dopants (i.e. MoO_x) from the MoS₂ surface [46, 47]. The optical image (inset in figure 4(e)) and the Raman spectra on the dendritic features (figure S12) show

optical contrast and spectrum of monolayer MoS₂, respectively. These results indicate that some 1L MoS₂ remain underneath the dendrites (MoO_x) and is not removed by the AFM tip.

Lastly, we annealed the partially cleaned flake at 400 °C for 3 h. As depicted in figure 4(f), the tip-cleaned regions (red dashed boxes in figure 4(e)) of the flake have been fully burned out, except for the flake edge and some residual nanoparticles. In contrast, a uniform layer with a thickness of ~0.8 nm (figures S10(g)–(i)) remains in the untouched region after annealing. Similarly, the ribbon edge of the remaining flake, which is between the red dotted line and the light blue dashed line (figure 4(d)), has an average height of ~0.8 nm. This value corresponds well with the thickness of monolayer MoO₃ crystal [48]. All of the flakes annealed at 400 °C for 3 h in our experiment are not visible through optical microscopy but are observable through AFM imaging (figure 3(e), figure 4(f)), in accordance with the pronounced chromism property of MoO₃ [49].

To provide direct proof of the resultant chemical composition changes of the annealed MoS₂ flakes, we conducted XPS measurements on both unannealed MoS₂ flakes and flakes that were first annealed at 240 °C for 3 h and then at 330 °C for 14 h. As shown in figures 5(a)–(c), the XPS spectra for all samples show the strong doublet of Mo⁴⁺ (shaded in pink) from MoS₂, which can be deconvoluted into Mo⁴⁺ 3d_{3/2} (232.6 ± 0.1 eV) and 3d_{5/2} (229.5 ± 0.2 eV) peaks [50, 51]; the peaks are highlighted in pink. For samples annealed at 240 °C, a weak Mo⁵⁺ state (shaded in purple) at 234.9 eV (3d_{3/2}) and 231.8 eV (3d_{5/2}) in the Mo 3d core line appears, suggesting the formation of the oxygen-deficient MoO_{3-x} [31, 52] or molybdenum oxysulfide MoO_xS_y [53, 54]. The Mo⁶⁺ species (shaded in red) at 236.2 eV (3d_{3/2}) and 233.2 eV (3d_{5/2}) show up in the sample annealed at 330 °C for 14 h, indicating that MoS₂ is partially oxidized. The percentage of the Mo⁶⁺ species is only about 22%, which is much lower compared to the values of the MoS₂ sample that was directly heated to 330 °C for 10 h [29] and heated at 320 °C for 10 min [47]. These findings suggest that the physical adsorption layer formed after annealing at 240 °C for 3 h contains little or no molybdenum oxides and with this layer on top, MoS₂ flakes become more stable under harsh annealing conditions. Additionally, the sulfur concentration acquired from the XPS spectra decreases from 67% (pristine) to 51% (240 °C 3 h) and to 38% (330 °C 14 h), suggesting that the density of sulfur vacancies increases with extended thermal annealing. Figures 5(d)–(f) demonstrates that the S 2p spectra remain almost unchanged between the pristine and annealed samples, but shift slightly to lower binding energies by about 0.1 eV, which may be attributed to the slight p-type doping [23]. This result is in good agreement with the observations from the Raman characterization that extended thermal annealing will increase the p-type doping level in MoS₂.

It is worth noting that the oxidation sensitivity of MoS₂ depends on its crystalline structure. The mechanically exfoliated MoS₂ are monocrystalline, while the chemically grown MoS₂ using chemical vapor deposition (CVD)

methods are polycrystalline with more S vacancies and grain boundaries. Mechanically exfoliated MoS₂ is thermally more stable than CVD-grown MoS₂, of which full oxidation reportedly occurs at 280 °C [55]. The use of a surface covering as a protective shield for the underlying TMD crystal against oxidation degradation is also reported for MoTe₂ [56].

2.3. Adsorption and oxidation of MoS₂ in dry air

With a better understanding of the role of the physical adsorption layer in the oxidation of MoS₂, we aim to understand its formation conditions. Pristine MoS₂ crystals are expected to thicken because of moisture adsorption in humid air [57, 58]. Hence, to confirm whether the height increase and formation of dendritic features result from the adsorption of ambient moisture, we tracked the morphology and layer thickness of thin MoS₂ flakes that were initially exfoliated during the summer (~55%–65% RH), stored in the open air for over six months (during which the humidity decreased to ~10% RH in the winter), then subjected to various annealing periods at 330 °C and multiple AFM tip-based cleanings.

After exposure to humid air for two months, the height of the 2L region increases by approximately 0.6 nm compared to the average height of a freshly annealed 2L flake (table S1), which is consistent with previous studies [57, 58]. However, the height decreases by 0.34 nm after being stored in relatively dry air. The evolution of the morphology, layer-thickness, and Raman spectra are shown in figures S14–15. Figures 6(a)–(c), (g) show that thermal annealing of this flake at 330 °C in dry air for 1 h and the following tip-based cleaning do not alter the flake thickness, in distinct contrast to the results obtained on flakes of the same number of layers, but annealed in the humid air. The Raman spectra in figure S15 show that the tip-based cleaning decreases the intensity and increases the FWHM of the A_{1g} and E_{2g}¹ modes, indicating disordering or amorphization of the MoS₂ crystal. Moreover, figure 6(f) shows that A_{1g} peak upshifts and narrows after the tip-based cleaning and annealing, suggesting more S vacancies induced by the annealing and cleaning. Figures 6(c)–(d) demonstrates that annealing at 330 °C for an extended duration severely oxidizes the flake that signs of sublimation and etching pits are visible on the 1L and 2L regions. Notably, the triangular etching pits appear after annealing at 330 °C for merely 6 h, in contrast to the 2L flake annealed in humid air that remains intact even after annealing for 14 h (figure 4(d)). The formation of etching pits might develop from the S defects generated by tip-based cleaning. These results suggest that, in the absence of the protection of the physical adsorption layers and the dendritic features, MoS₂ is prone to oxidation at 330 °C in dry air. Additionally, the tip-based cleaning results in an accumulation of MoS₂ and molybdenum oxides debris at the end of each scan line (figure S16).

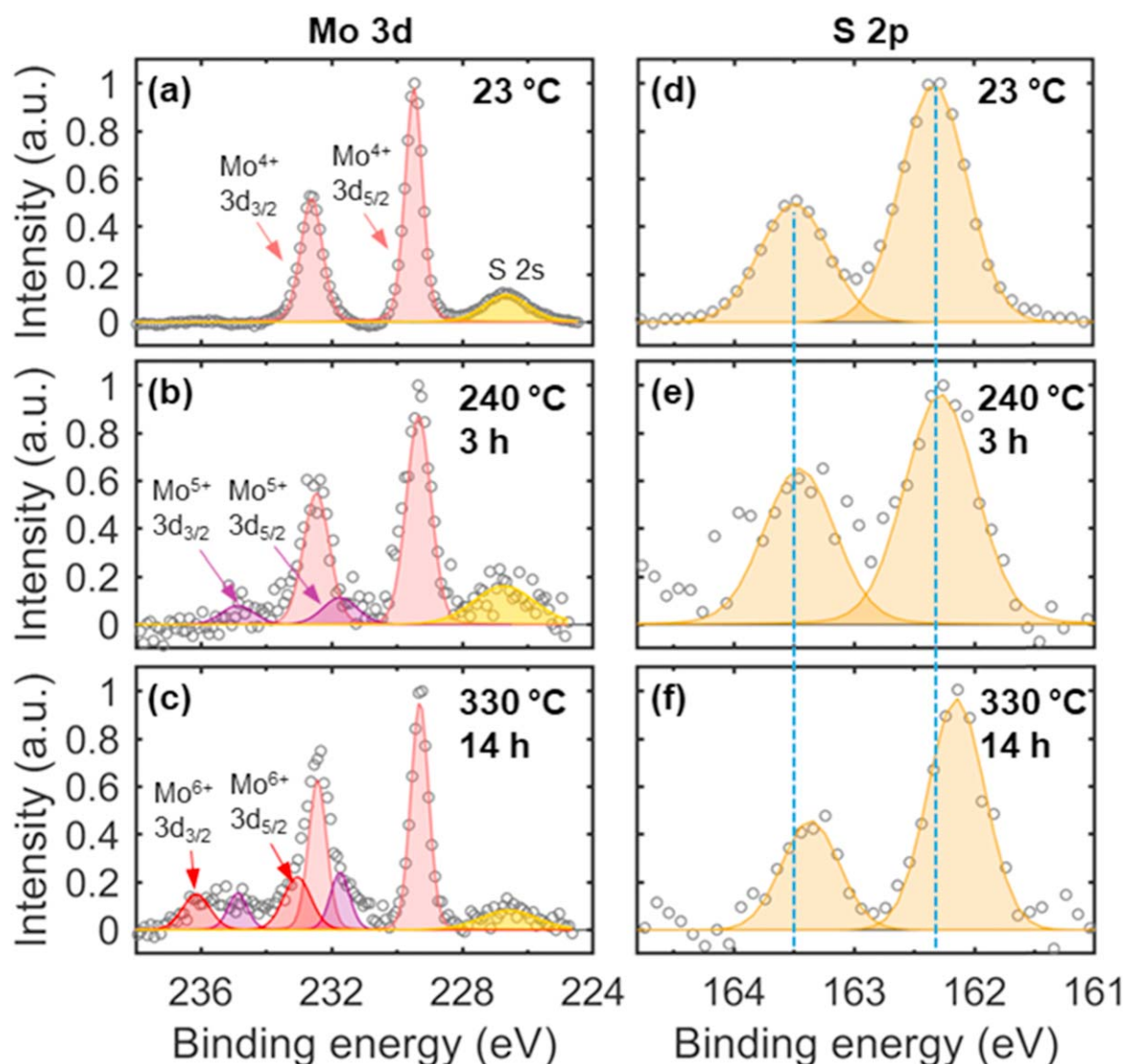


Figure 5. XPS spectra of (a)–(c) Mo 3d with S 2s, and (d)–(f) S 2p core levels measured from pristine samples (23 °C), and from samples annealed at 240 °C for 3 h, 330 °C for 14 h in air with ~60% RH.

3. Conclusions

In summary, the oxidation of mono- or few-layer MoS₂ flakes in the air under a wide range of annealing temperatures and humidities is investigated. Our findings reveal, *for the first time*, the formation of a uniform nanometer-thick physical adsorption layer on the basal plane of atomically thin MoS₂ through moisture adsorption during low-temperature thermal annealing. The physical adsorption acts as a thermal shield for the underlying MoS₂ lattices and does not induce straining, thus having no direct effect on its electrical properties. Furthermore, the physical adsorption is fully removable using facile annealing at 400 °C or through AFM tip-based cleaning. Chemical adsorption of oxygen molecules on sulfur vacancies leads to p-type doping of MoS₂ and phase transformation from MoS₂ to MoO_x, and the resulting ice-like dendritic features are hard to remove by either thermal annealing or AFM tip-based cleaning.

The findings of the physical and chemical adsorption phenomena provide critical insights into the oxidation

mechanism of atomically thin MoS₂ and highlight the importance of humidity control in ensuring reliable and optimal performance for MoS₂-based devices. These findings have important implications for the understanding and ultimately a full command and control of fundamental physical and chemical properties of MoS₂, which are critical to the pursuits of its applications. For example, the protective role of the physical adsorption layer is instrumental to the preservation of the pristine crystal lattice structure of MoS₂ and its intrinsic physical properties from contamination or in harsh thermal environments. This surface engineering approach is, in particular, important to their electronics applications, where elevated thermal heating is often involved in the manufacturing and operation of the device. The induction of S-vacancies in MoS₂ by AFM-tip cleaning is a promising and facile venue for controllable defect engineering in 2D-TMD that can be used toward strain engineering, bandgap engineering, and electrochemical catalyzing [8–10]. The reported experimental findings may help stimulate further theoretical study to better understand the physico-chemisorption

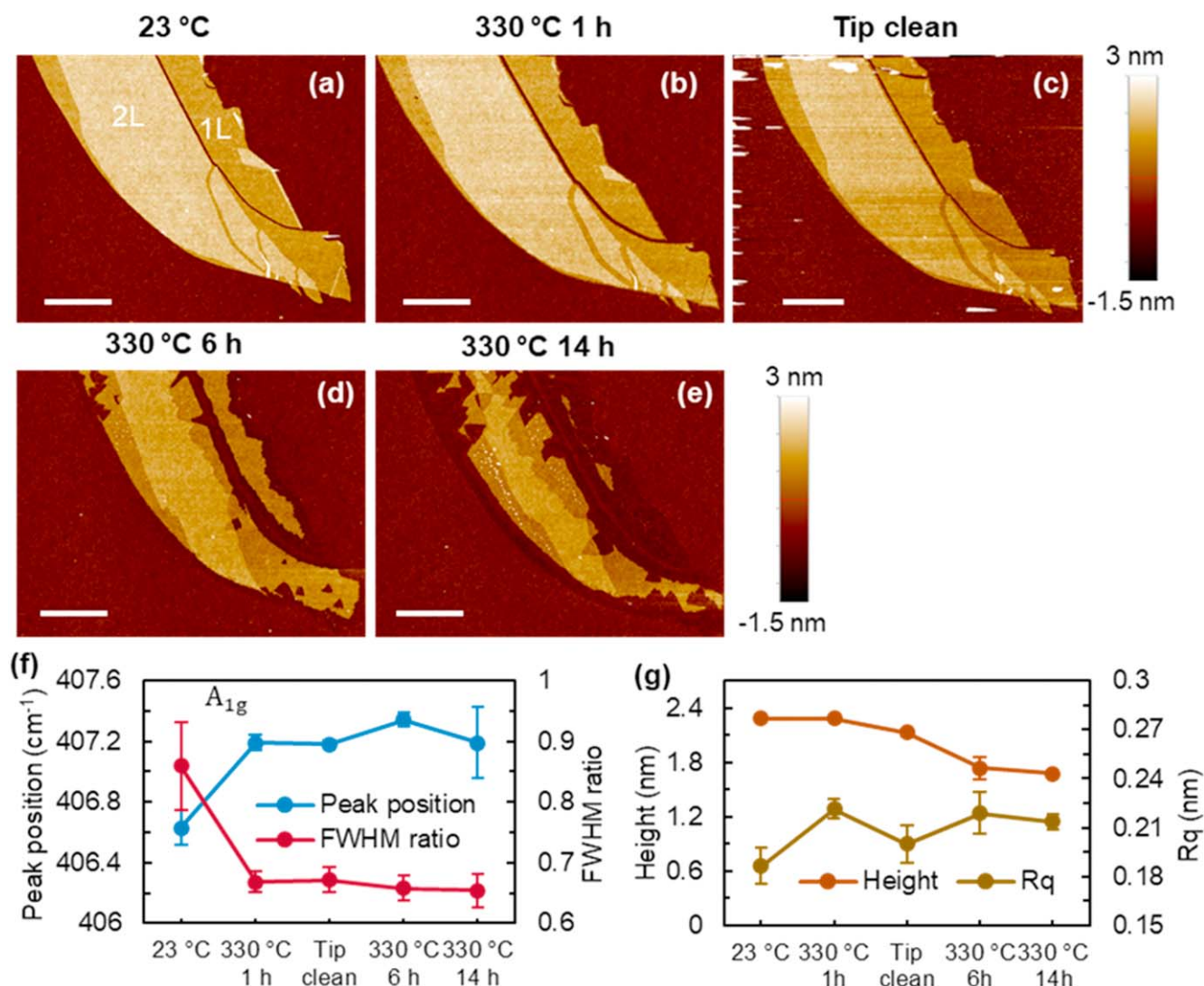


Figure 6. Thermal annealing of a 1L–2L MoS₂ flake in the air at 330 °C with ~10% RH and AFM tip-based cleaning. AFM topographic image of the flake (a) before annealing, (b), (c) after annealing at 330 °C for 1 h and AFM tip-based cleaning, (d), (e) annealing at 330 °C for 6 h and 14 h. Scale bar, 2 μm. (f) A_{1g} mode peak position and FWHM ratio of the 2L region measured before annealing, after annealing, and tip-based cleaning. (g) The thickness and surface roughness of the 2L region. The error bars in f and g are standard deviation of measurements at three to four different locations on the 2L region.

phenomena in the thermal oxidation of MoS₂, in particular, at the atomistic level with the aid of advanced computational tools, such as molecular dynamics simulations and density-functional theory calculations [59–61]. These advances are also relevant to the study of other TMDs (e.g. MoTe₂ and MoSe₂ [56, 62] that are sensitive to the ambient environment and ultimately contribute to the development of the next-generation cutting edge 2D-TMD based electronics and devices with optimal design and performance.

4. Methods

4.1. Preparation of mono- and few-layer MoS₂ flakes

Mono- and few-layer MoS₂ flakes were mechanically exfoliated from bulk MoS₂ crystal (SPI supplies) onto a Si substrate with a 285 nm SiO₂ layer (Graphene Supermarket),

using Scotch tape as the transfer media. No heating or post-annealing was involved during mechanical exfoliation or for removing tape residue.

4.2. Thermal annealing

Thermal annealing was conducted on stand-alone mechanically exfoliated MoS₂ flakes on SiO₂/Si substrates (5 mm by 5 mm) in a ceramic crucible of a TS1500 heating stage programmed by a T96 system controller (Linkam Scientific Instruments). The temperature of the sample was monitored using a PT100 platinum sensor with a resolution of 0.01 °C.

The humidity was monitored by a temperature-compensated humidity sensor (Model 554, Electro-Tech Systems, Inc.). After the characterization of the MoS₂ flakes at room temperature, the sample was heated to 50 °C with a ramp rate of 5 °C min⁻¹, held for 15 min, then cooled to room temperature at the same rate, followed by Raman and AFM

measurements. Subsequently, the same sample was heated to a temperature 50 °C higher than the former one using the same procedure, followed by the same characterization routine.

4.3. Characterizations

All AFM measurements and tip-based cleaning were conducted using a Park XE 70 AFM (Park Systems). The scanners were calibrated, and the details are shown in figure S17. The topography of the MoS₂ flakes before and after annealing was inspected by NCM AFM with a regular silicon cantilever (Tap300Al-G, Budget Sensors) which had a nominal spring constant of 40 N m⁻¹. The measurement configuration of the NCM imaging is discussed in figure S18. For contact mode imaging, we used a soft cantilever (csg01, NT-MDT spectrum instruments) with a spring constant ranging from 0.003 to 0.130 N m⁻¹, to eliminate the tip-induced scratches on the sample. Tip-based-cleaning was conducted with a contact mode cantilever (csg10, NT-MDT spectrum instruments) with a spring constant ranging from 0.010 to 0.500 N m⁻¹. The spring constant of each cantilever was calibrated by using the Sader method [63].

Raman spectroscopy measurements were performed with a Renishaw inVia Reflex Raman microscope equipped with a 532 nm laser excitation with 2400 lines/mm grating. The spectra were collected through a 100X objective lens with an N.A. of 0.85. The laser power was kept below 0.5 mW to avoid the heating effect. Raman spectra were calibrated by using a bulk monocrystalline Si to peak position at 520.5 cm⁻¹.

X-ray photoelectron spectroscopy measurements were conducted with PHI VersaProbe II. All spectra were taken using monochromatic Al K α radiation ($h\nu = 1486.6$ eV at 48.3 W) with a beam diameter of 200 μ m. Adventitious carbon C 1s (C–C and C–H at 284.8 eV) was used for charge correction referencing. Curve fitting was performed using a mixed Gaussian-Lorentzian function after a Shirley background subtraction. An area ratio of 3:2 between the Mo 3d_{3/2} and 3d_{5/2} was used in the fitting.

Acknowledgments

This work was partially supported by the National Science Foundation under Grant No. NSF-CMMI 2006127.

Data availability statement

The data that support the findings of this study are available upon reasonable request from the authors.

ORCID iDs

Yingchun Jiang  <https://orcid.org/0000-0001-5571-4201>
 Zihan Liu  <https://orcid.org/0009-0006-9279-1162>
 Changhong Ke  <https://orcid.org/0000-0002-5170-9859>

References

- [1] Radisavljevic B, Radenovic A, Brivio J, Giacometti V and Kis A 2011 Single-layer MoS₂ transistors *Nat. Nanotechnol.* **6** 147–50
- [2] Wang Q H, Kalantar-Zadeh K, Kis A, Coleman J N and Strano M S 2012 Electronics and optoelectronics of two-dimensional transition metal dichalcogenides *Nat. Nanotechnol.* **7** 699–712
- [3] Jiang Y, Sridhar S, Liu Z, Wang D, Zhou H, Deng J, Chew H B and Ke C 2023 The interplay of intra- and inter-layer interactions in bending rigidity of ultrathin 2D materials *Appl. Phys. Lett.* **122** 1–8153101
- [4] Amani M *et al* 2015 Near-unity photoluminescence quantum yield in MoS₂ *Science (80-)* **350** 1065–8
- [5] Yin Z, Li H, Li H, Jiang L, Shi Y, Sun Y, Lu G, Zhang Q, Chen X and Zhang H 2012 Single-layer MoS₂ photo-transistors *ACS Nano* **6** 74–80
- [6] Perkins F K, Friedman A L, Cobas E, Campbell P M, Jernigan G G and Jonker B T 2013 Chemical vapor sensing with monolayer MoS₂ *Nano Lett.* **13** 668–73
- [7] Li H, Yin Z, He Q, Li H, Huang X, Lu G, Fam D W H, Tok A I Y, Zhang Q and Zhang H 2012 Fabrication of single- and multilayer MoS₂ film-based field-effect transistors for sensing NO at room temperature *Small* **8** 63–7
- [8] Liu D, Bian Y, Zhu Z, Shao Y and Li M 2022 Detection of trace water based on electro-oxidation of molybdenum disulfide nanomaterials to form molybdenum oxysulfide *ACS Appl. Mater. Interfaces* **14** 23850–8
- [9] Ma Y, Leng D, Zhang X, Fu J, Pi C, Zheng Y, Gao B, Li X, Li N, Chu P K, Luo Y and Huo K 2022 Enhanced activities in alkaline hydrogen and oxygen evolution reactions on MoS₂ electrocatalysts by in-plane sulfur defects coupled with transition metal doping *Small* **18** 2203173
- [10] Wang Z *et al* 2018 Controllable etching of MoS₂ basal planes for enhanced hydrogen evolution through the formation of active edge sites *Nano Energy* **49** 634–43
- [11] Sim D M, Kim M, Yim S, Choi M, Choi J, Yoo S and Jung Y S 2015 Controlled doping of vacancy-containing few-layer MoS₂ via highly stable thiol-based molecular chemisorption *ACS Nano* **9** 12115–23
- [12] Mak K F, McGill K L, Park J and McEuen P L 2014 The valley hall effect in MoS₂ transistors *Science (80-)* **344** 1489–92
- [13] Yalon E *et al* 2017 Energy dissipation in monolayer MoS₂ electronics *Nano Lett.* **17** 3429–33
- [14] Park W, Park J, Jang J, Lee H, Jeong H, Cho K, Hong S and Lee T 2013 Oxygen environmental and passivation effects on molybdenum disulfide field effect transistors *Nanotechnology* **24** 095202
- [15] Qiu H, Pan L, Yao Z, Li J, Shi Y and Wang X 2012 Electrical characterization of back-gated bi-layer MoS₂ field-effect transistors and the effect of ambient on their performances *Appl. Phys. Lett.* **100** 123104
- [16] Tagawa M, Muromoto M, Hachiue S, Yokota K, Ohmae N, Matsumoto K and Suzuki M 2005 Hyperthermal atomic oxygen interaction with MoS₂ lubricants and relevance to space environmental effects in low Earth orbit—effects on friction coefficient and wear-life *Tribol. Lett.* **18** 437–43
- [17] Chuang S *et al* 2014 MoS₂ P-type transistors and diodes enabled by high work function MoO₃ contacts *Nano Lett.* **14** 1337–42
- [18] Neal A T, Pachter R and Mou S 2017 P-type conduction in two-dimensional MoS₂ via oxygen incorporation *Appl. Phys. Lett.* **110** 193103
- [19] Yang S, Wang Z, Hu Y, Luo X, Lei J, Zhou D, Fei L, Wang Y and Gu H 2015 Highly responsive room-temperature hydrogen sensing of α -MoO₃ nanoribbon membranes *ACS Appl. Mater. Interfaces* **7** 9247–53

- [20] Ji F, Ren X, Zheng X, Liu Y, Pang L, Jiang J and Liu S 2016 2D-MoO₃ nanosheets for superior gas sensors *Nanoscale* **8** 8696–703
- [21] Jaramillo T F, Jørgensen K P, Bonde J, Nielsen J H, Horch S and Chorkendorff I 2007 Identification of active edge sites for electrochemical H₂ evolution from MoS₂ nanocatalysts *Science (80-)* **317** 100–2
- [22] Azcatl A et al 2016 Covalent nitrogen doping and compressive strain in MoS₂ by remote N₂ plasma exposure *Nano Lett.* **16** 5437–43
- [23] Zhu H, Qin X, Cheng L, Azcatl A, Kim J and Wallace R M 2016 Remote plasma oxidation and atomic layer etching of MoS₂ *ACS Appl. Mater. Interfaces* **8** 19119–26
- [24] Ukegbu U and Szoszkiewicz R 2019 Microscopic kinetics of heat-induced oxidative etching of thick MoS₂ crystals *J. Phys. Chem. C* **123** 22123–9
- [25] Zhou H et al 2013 Thickness-dependent patterning of MoS₂ sheets with well-oriented triangular pits by heating in air *Nano Res.* **6** 703–11
- [26] Neupane G P, Dhakal K P, Kim H, Lee J, Kim M S, Han G, Lee Y H and Kim J 2016 Formation of nanosized monolayer MoS₂ by oxygen-assisted thinning of multilayer MoS₂ *J. Appl. Phys.* **120** 1–6
- [27] Yamamoto M, Einstein T L, Fuhrer M S and Cullen W G 2013 Anisotropic etching of atomically thin MoS₂ *J. Phys. Chem. C* **117** 25643–9
- [28] Tang J, Wei Z, Wang Q, Wang Y et al 2020 *In situ* oxygen doping of monolayer MoS₂ for novel electronics *Small* **16** 2004276
- [29] Wu J, Li H, Yin Z, Li H, Liu J, Cao X, Zhang Q and Zhang H 2013 Layer thinning and etching of mechanically exfoliated MoS₂ nanosheets by thermal annealing in air *Small* **9** 3314–9
- [30] Nan H et al 2014 Strong photoluminescence enhancement of MoS₂ through defect engineering and oxygen bonding *ACS Nano* **8** 5738–45
- [31] Yoon A, Kim J H, Yoon J, Lee Y and Lee Z 2020 Van der waals epitaxial formation of atomic layered α -MoO₃ on MoS₂ by oxidation *ACS Appl. Mater. Interfaces* **12** 22029–36
- [32] Park S et al 2021 Operando study of thermal oxidation of monolayer MoS₂ *Adv. Sci.* **8** 2002768
- [33] Tongay S, Zhou J, Ataca C, Liu J, Kang J, Matthews T, You L, Li J, Grossman J and Wu J 2013 Broad-Range Modulation of Light Emission in Two-Dimensional Semiconductors by Molecular Physisorption Gating *Nano Lett.* **13** 2831–2836
- [34] Shu H, Li Y, Niu X and Wang J 2016 Greatly enhanced optical absorption of a defective MoS₂ monolayer through oxygen passivation *ACS Appl. Mater. Interfaces* **8** 13150–6
- [35] Spychalski W L, Pisarek M and Szoszkiewicz R 2017 Microscale insight into oxidation of single MoS₂ crystals in air *J. Phys. Chem. C* **121** 26027–33
- [36] Sitek J, Plocharski J, Pasternak I, Gertych A P, Mcaliese C, Conran B R, Zdrojek M and Strupinski W 2020 Substrate-induced variances in morphological and structural properties of MoS₂ Grown by chemical vapor deposition on epitaxial graphene and SiO₂ *ACS Appl. Mater. Interfaces* **12** 45101–10
- [37] Wang X, Fan W, Fan Z, Dai W, Zhu K, Hong S, Sun Y, Wu J and Liu K 2018 Substrate modified thermal stability of mono- and few-layer MoS₂ *Nanoscale* **10** 3540–6
- [38] Hong J et al 2015 Exploring atomic defects in molybdenum disulfide monolayers *Nat. Commun.* **6** 1–8
- [39] Chakraborty B, Bera A, Muthu D V S, Bhowmick S, Waghmare U V and Sood A K 2012 Symmetry-dependent phonon renormalization in monolayer MoS₂ transistor *Phys. Rev.* **85** 2–5 B
- [40] Pető J, Ollár T, Vancsó P, Popov Z I, Magda G Z, Dobrik G, Hwang C, Sorokin P B and Tapasztó L 2018 Spontaneous doping of the basal plane of MoS₂ single layers through oxygen substitution under ambient conditions *Nat. Chem.* **10** 1246–51
- [41] Conley H J, Wang B, Ziegler J I, Haglund R F, Pantelides S T and Bolotin K I 2013 Bandgap engineering of strained monolayer and bilayer MoS₂ *Nano Lett.* **13** 3626–30
- [42] Li H, Zhang Q, Yap cc R, Tay B K, Edwin T H T, Olivier A and Baillargeat D 2012 From bulk to monolayer MoS₂: evolution of raman scattering *Adv. Funct. Mater.* **22** 1385–90
- [43] Lee C, Yan H, Brus L E, Heinz T F, Hone J and Ryu S 2010 Anomalous lattice vibrations of single- and few-layer MoS₂ *ACS Nano* **4** 2695–700
- [44] Castellanos-Gomez A, Barkelid M, Goossens A M, Calado V E, Van Der Zant H S J and Steele G A 2012 Laser-thinning of MoS₂: on demand generation of a single-layer semiconductor *Nano Lett.* **12** 3187–92
- [45] Nemanich R J, Solin S A and Martin R M 1981 Light scattering study of boron nitride microcrystals *Phys. Rev. B* **23** 6348–56
- [46] Rogala M, Sokołowski S, Ukegbu U, Mierzwa A and Szoszkiewicz R 2021 Direct identification of surface bound MoO₃ on single MoS₂ flakes heated in dry and humid air *Adv. Mater. Interfaces* **8** 1–11
- [47] Szoszkiewicz R, Rogala M, Paweł D and Abrowski 2020 Surface-bound and volatile mo oxides produced during oxidation of single MoS₂ crystals in air and high relative humidity *Materials (Basel)* **2** 3067
- [48] Kalantar-zadeh K et al 2010 Synthesis of nanometre-thick MoO₃ sheets *Nanoscale* **2** 429–33
- [49] de Castro I A, Datta R S, Ou J Z, Castellanos-Gomez A, Sriram S, Daeneke T and Kalantar-zadeh K 2017 Molybdenum oxides—from fundamentals to functionality *Adv. Mater.* **29** 1–31
- [50] Brown N M D, Cui N and Mckinley A 1998 An XPS study of the surface modification of natural MoS₂ following treatment in an RF-oxygen plasma *Applied Surface Science* **134** 11–21
- [51] Baker M A, Gilmore R, Lenardi C and Gissler W 1999 XPS investigation of preferential sputtering of S from MoS₂ and determination of MoS_x stoichiometry from Mo and S peak positions *Appl. Surf. Sci.* **150** 255–62
- [52] Ko T Y, Jeong A, Kim W, Lee J, Kim Y, Lee J E et al 2017 On-stack two-dimensional conversion of MoS₂ into 2D *Mater.* **4** 014003
- [53] Bessonov A A, Kirikova M N, Petukhov D I, Allen M, Ryhänen T and Bailey M J A 2015 Layered memristive and memcapacitive switches for printable electronics *Nat. Mater.* **14** 199–204
- [54] Jung C, Yang H I and Choi W 2019 Effect of ultraviolet-ozone treatment on MoS₂ monolayers: comparison of chemical-vapor-deposited polycrystalline thin films and mechanically exfoliated single crystal flakes *Nanoscale Res. Lett.* **14** 1–8
- [55] Ren S, Shi Y, Zhang C, Cui M and Pu J 2022 Anomalous enhancement oxidation of few-layer MoS₂ and MoS₂/h-BN heterostructure *Nano Res.* **15** 7081–90
- [56] Pham T T, Castellino R, Felten A and Sporken R 2022 Study of surface oxidation and recovery of clean MoTe₂ films *Surf. Interfaces* **28** 101681
- [57] Xiao C, Shi P, Yan W, Chen L, Qian L and Kim S H 2019 Thickness and structure of adsorbed water layer and effects on adhesion and friction at nanoasperity contact *Colloids Interfaces* **3** 1–31
- [58] Arif T, Yadav S, Colas G, Singh C V and Filleter T 2019 Understanding the independent and interdependent role of water and oxidation on the tribology of ultrathin molybdenum disulfide (MoS₂) *Adv. Mater. Interfaces* **6** 1–9
- [59] Farigliano L M, Paredes-Olivera P A and Patrino E M 2020 Initial steps of oxidative etching of MoS₂ basal plane induced by O₂ *J. Phys. Chem. C* **124** 13177–86

- [60] Akdim B, Pachter R and Mou S 2016 Theoretical analysis of the combined effects of sulfur vacancies and analyte adsorption on the electronic properties of single-layer MoS₂ *Nanotechnology* **27** 185701
- [61] Longo R C, Addou R, Kc S, Noh J, Smyth C M, Barrera D, Zhang C, Hsu J W P, Wallace R M and Cho K 2017 Intrinsic air stability mechanisms of two-dimensional transition metal dichalcogenide surfaces: basal versus edge oxidation *2D Mater.* **4** 025050
- [62] Mirabelli G *et al* 2016 Air sensitivity of MoS₂, MoSe₂, MoTe₂, HfS₂, and HfSe₂ *J. Appl. Phys.* **120** 125102
- [63] Sader J E, Chon J W M and Mulvaney P 1999 Calibration of rectangular atomic force microscope cantilevers *Rev. Sci. Instrum.* **70** 3967–9